Iranian Journal of Chemical Engineering
Vol. 15, No. 1 (Winter 2018), IAChE

Dynamic Behavior of an Oil Droplet Adhered to the Wall Surface in a Channel Flow by the Lattice Boltzmann Method

M. Varmazyar [1*], R. Mohamady [2], M. Bazargan [2]

[1] Department of Mechanical Engineering, Shahid Rajaee Teacher Training University, P. O. Box: 16788-15811, Tehran, Iran
[2] Department of Mechanical Engineering, K. N. Toosi University of Technology, P. O. Box: 19914-3344, Tehran, Iran

ARTICLE INFO

Article history:
Received: 2016-11-06
Accepted: 2017-01-10

Keywords:
Lattice Boltzmann Method
Multi-Component Fluid
Droplet Behavior
Critical Shear Rate
Capillary Number
Detachment and Crawling

ABSTRACT

The Lattice Boltzmann Method is used to simulate the dynamics of droplet deformation in a channel flow under various conditions. The droplet behavior has been investigated under transient conditions. For cases where the droplet remains attached to the surface, the shape deformation of the droplet during crawling is captured. It has been shown that there is a limiting value for the droplet volume beyond which the critical shear rate remains almost constant and does not demonstrate much correlation with the size of the droplet. The predicted shapes of the droplet at various stages of deformation in the course of the flow by the current LBM code demonstrate more resemblance to the reported experiments than those obtained by a traditional CFD code. The effects of the droplet's initial volume and Reynolds number on the detachment and crawling processes are also investigated. The results are presented at various time steps to better demonstrate the droplet separation. Under the flow conditions investigated, wherever the Aniline droplet detaches, the entire droplet separates from the surface. For an Isoquinoline droplet however, once the main body is detached, a small part of the droplet remains attached to the surface in flows with low Reynolds numbers.

1. Introduction

One of the most powerful and newest methods in numerical simulation of fluid flows is the Lattice Boltzmann Method (LBM). The LBM is a kinetic method which is based on the Integro-differential Boltzmann equation. The fundamental idea of Boltzmann's equation is that a fluid is composed of interacting particles whose behavior can be described by classical mechanics. From a macroscopic point of view, a certain volume of a fluid contains a very large number of particles. Thus, a statistical treatment is necessary and appropriate. The inter-relation between the particles of the fluid can be explained simply by the streaming in space and elastic collision interactions. The main advantage associated with the LBM is the

*Corresponding author: varmazyar.mostafa@srttu.edu

ease of simulating complex flows [1-4]. The LBM presents a simple solution for simulating multi-phase and multi-component fluid flows that are more difficult to solve by other methods. That is because the non-linear Navier-Stokes equations in conventional methods are replaced by the semi-linear Boltzmann equation. Furthermore, the parallelization techniques are highly fitted to the LBM.

One of the problems which seems to be interesting to be studied by the LBM is the dynamic behavior of a droplet adhering to the surface of a wall subject to a flow over the surface. Some applications of this study include the formation of emulsions by cross-flow of two immiscible fluids [5], the detachment of the droplet from the stainless steel surface [6], the removal of the droplet from the solid surface [7], the deformation of the water droplet under influence of oxygen flow in fuel cells [8], and the deformation and detachment of the droplet to mimic a biological cell in the medical field [9].

The droplet deformation consists of three stages namely droplet sliding, droplet crawling, and droplet detachment. Most of the previous studies are focused on the droplet detachment process and the influence of corresponding system parameters. For example, Dimitrakopoulos et al. [10] studied the detachment of a two-dimensional droplet which adheres to the solid surface in a sheared flow without neglecting the gravity effect. They showed that the critical shear rates associated with the onset of droplet detachment depends on the capillary number ($Ca=\mu U/\gamma$, a ratio of viscous to surface tension forces) and the initial shape of the droplet. Ding and Spelt [11] used a numerical simulation model and obtained the droplet shape under different conditions of moderate Reynolds numbers, initial droplet shapes, and contact angles. Their results were in good agreement with the optimal droplet shapes predicted by Dimitrakopoulos et al. [10] for the crawling flow.

Mahe et al. [12] studied the critical shear rates required for the detachment of oil droplets with different sizes. They realized that the droplets with bigger initial volumes need a smaller shear rate to detach from the wall surface. Based on the observations of Mahe et al. [12], Basu et al. [13] proposed a mathematical model for the detachment process of a droplet. Their mathematical model predicted a reasonable critical shear for the detachment of a droplet with different equilibrium contact angles. The deformation of oil droplets with different viscosity adhering to the surface of the solid wall in a rectangular channel induced by a pressure-driven, laminar flow of water was experimentally studied by Seevaratnam et al. [14]. They analyzed the effects of initial droplet volume, flow rate, and viscosity ratio on the various modes of droplet motion and deformation. They expressed the critical conditions for droplet ‘sliding’, ‘crawling’ and detachment from the wall surface as a function of system parameters. Dussan [15] developed a yield criterion for critical capillary number as a function of advancing and receding contact angles, and found that contact angle hysteresis increases with the increase of capillary and Reynolds numbers.

Hao and Cheng [16] used the multi-phase free-energy lattice Boltzmann method to analyze the water droplet deformation and the shape of the droplet at different times and conditions. They presented the dynamics of the water droplet deformation in all steps of the droplet's movements in the gas flow channel. They also calculated the size of the detached

droplet and the time it takes for the droplet to leave the channel. Their results showed that a larger *Ca* number leads to a faster removal of the water droplet. Gupta and Basu [17] studied an oil droplet's deformation on a solid surface in simple shear flow by employing a computational fluid dynamics tool (Fluent 6.3). They neglected the inertial and gravitational forces and validated their numerical predictions for the shape of the oil droplet with their own experiments. They revealed that oil droplet deformation increases with an increase in the capillary number, Reynolds number, and size of the oil droplet.

In this study, the LBM is employed to investigate the flow of two immiscible fluids. The inter particle forces in the interface of two fluids are calculated by means of a simple equation. The inertial and gravitational forces are assumed to be negligible. The deformation of a droplet occurs continuously in several stages along the course of flow. Some of the important stages of droplet deformation like crawling and detachment processes for two different oil droplets (Aniline and Isoquinoline) and the influence of some system parameters on the droplet deformation process are investigated. At first, the droplet starts to deform and slides while it keeps adhering to the wall. The effects of the initial volume of the droplet and the flow Reynolds number on the crawling process are investigated. Under certain circumstances, for example, upon the sufficient growth of the Reynolds number, the droplet leaves the wall and remains in the fluid flow. To better determine the flow conditions leading to the detachment, the critical shear rate in the channel associated with the onset of the droplet taking off from the wall surface is also calculated.

2. Model specification

Error! Reference source not found. shows a schematic of the model used in this study. An oil droplet which is adhered to the wall of a rectangular channel flow of water has been considered in a two-dimensional frame.

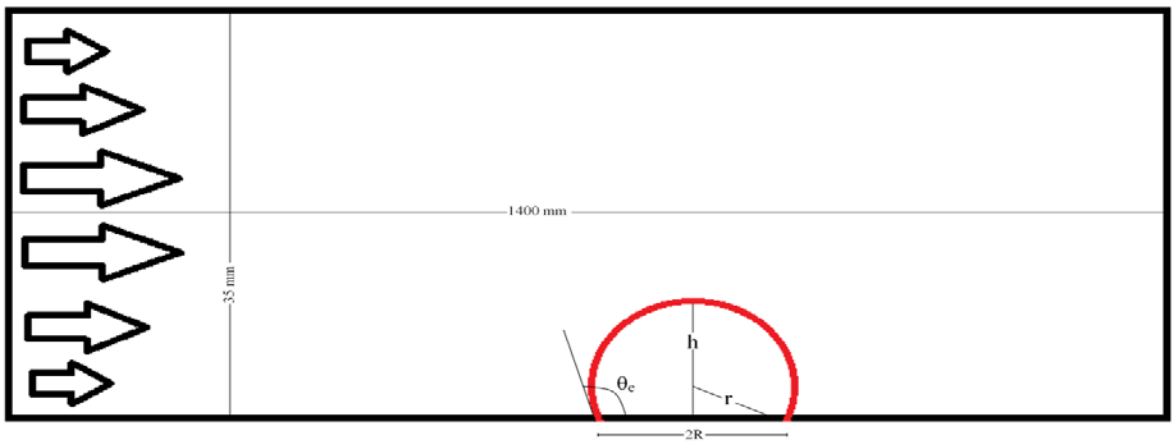

Figure 1. Schematic of a droplet adhered to the wall (The origin is located on the left bottom corner of the duct).

The volume of droplet V is assumed to be equal to the volume of a sphere with radius R defined as:

$$R = r/\sin\theta_e \quad (1)$$

where r is the contact radius, and θ_e is the contact angle between the droplet and solid surface:

$$\theta_e = 2\tan^{-1} h/2R \quad (2)$$

The density and viscosity of water are denoted as ρ_1 and μ_1. The oil droplet has density ρ_2 and viscosity μ_2. The Bound number is defined as below:

$$Bo=(\rho_2-\rho_1)gR^2/\gamma \quad (3)$$

where g is the gravity acceleration and γ is the interfacial tension between oil and water. Both the water flow and the oil droplet are considered to be Newtonian fluids. The Bound number is assumed to be less than 1 and the buoyancy effects can be neglected. The channel size is 35×1400 mm^2. The properties of the fluids as well as the oil-water interfacial tensions are given in **Error! Reference source not found.**. Two different fluids, Aniline and Isoquinoline, have been considered for the oil droplet.

Table 1
Properties of Fluids [17].

Fluids	Density ρ (kg/m^2)	Viscosity μ (pas)	Oil-water interfacial tension γ (mN/m)
Water	988.0	0.001	-
Aniline	1023.5	0.0034	5.27
Isoquinoline	1099.0	0.0029	0.6

3. Lattice Boltzmann method

There are several ways in the LBM to simulate the behavior of the oil droplet in the flow. The examples include the model of Shan and Chen [18], the level set technique [19], and the free energy method [16]. The Shan and Chen Method has been implemented in this study. The other two methods are usually used in simulating the multi-component systems where the viscosity and density ratios of two fluids are large. The method of Shan and Chen [20] is more applicable and robust to calculate the intermolecular and volumetric forces in the flow. As the first step, the distribution functions are required to be defined. A distribution function at each node specifies the probability of the particle motion in specified directions. In the current study, a D2Q9 model has been used which considers nine directions in a two-dimensional space. Figure 1 shows the velocity directions (e_a) for a particle in a D2Q9 lattice.

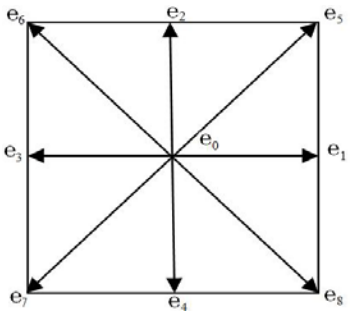

Figure 1. The velocity directions for a D2Q9 Lattice model.

The next step is to determine the collision model. The collision model is the main parameter deciding how the distribution function varies at each node during the

diffusion step. The Bhatnagher, Gross and Krook (BGK) [21] proposed a formulation to simplify the collision integral relation. The Navier-Stokes equation can be derived by using the Chapman-Enskog analysis and making the BGK assumption. The BGK collision parameter often appears to be adequate for simple systems and is defined as follows:

$$\Omega_a = \frac{1}{\tau^\sigma}[f_a^\sigma(x,t) - f_a^{\sigma,eq}(x,t)] \qquad (4)$$

where σ is related to the components of the fluid, $f_a^\sigma(x,t)$ is the distribution function of each component, a is the index representing the direction of velocity defined in the lattice model, and τ^σ is the relaxation time due to the kinematic viscosity. In the current study, the relaxation time is defined as follows:

$$\tau^\sigma = 3\upsilon^\sigma + \frac{1}{2} \qquad (5)$$

The streaming and collision steps can be simulated for each component of the fluid by the following equation:

$$f_a^\sigma(x + e_a\Delta t, t + \Delta t) = f_a^\sigma(x,t) - \frac{1}{\tau_\sigma}[f_a^\sigma(x,t) - f_a^{\sigma,eq}(x,t)] \qquad (6)$$

The equilibrium distribution function $f_a^{\sigma,eq}(x,t)$ can be calculated as follows:

$$f_a^{\sigma,eq}(x) = w_a\rho^\sigma(x)[1 + 3\frac{e_a.u^{\sigma,eq}}{{c_s}^2} + \frac{9}{2}\frac{(e_a.u^{\sigma,eq})^2}{{c_s}^4} - \frac{3}{2}\frac{{u^{\sigma,eq}}^2}{{c_s}^2}] \qquad (7)$$

where c_s is the speed of sound, and w_i is the corresponding equilibrium density for $\vec{u}^{eq} = 0$. Macroscopic velocity $u^{\sigma,eq}$ is given by:

$$u^{\sigma,eq} = u' + \frac{\tau^\sigma F^\sigma}{\rho^\sigma} \qquad (8)$$

where F^σ is the force acting on the component denoted by σ. It includes the fluid-fluid cohesion F_c^σ, fluid-solid adhesion F_{ads}^σ, and body force F_b, i.e., $F^\sigma = F_c^\sigma + F_{ads}^\sigma + F_b$. Moreover, in Eq. (8), u' is called the common velocity and is defined as follows:

$$u' = \sum_{\sigma=1}^{s}\frac{\rho^\sigma u^\sigma}{\tau^\sigma} \Big/ \sum_{\sigma=1}^{s}\frac{\rho^\sigma}{\tau^\sigma} \qquad (9)$$

where the macroscopic fluid density and velocity can be calculated using the distribution functions as follows:

$$\rho^\sigma = \sum_{a=0}^{8} f_a \quad , \quad u^\sigma = \frac{1}{\rho^\sigma}\sum_{a=0}^{8} f_a e_a \qquad (10)$$

3.1. Fluid-fluid cohesion

The cohesive force between two fluids seems to be the dominant component in the problem under consideration in this study. The cohesive force acting on the σ^{th} component is defined as:

$$F_{ads,c}^\sigma(x,t) = -G_c\rho^\sigma(x,t)\sum_a w_a\rho^{\tilde{\sigma}}(x + e_a\Delta t, t)e_a \qquad (11)$$

where σ and $\tilde{\sigma}$ denote two different fluid components and G_c is the Green function. The extent of the cohesion force can be controlled by the value of the Green function. The Green

function is related to the mass diffusion and controls the interface thickness between two fluids. By increasing the value of the Green function, the interface layer will become narrow and may eventually make the solution unstable. Such a limiting value is defined as follows: $G_c=1/(\rho^1+\rho^2)$.

3.2. Fluid-solid adhesion

The force acting on either fluid by the wall surfaces can be computed as follows:

$$F_{ads}^{\sigma}(x,t) = -G_{ads}^{\sigma}\rho^{\sigma}(x,t)\sum_{a} w_a S(x+e_a\Delta t,t)e_a \quad (12)$$

Herein, $S(x+e_a\Delta t,t)$ is an indicator function taking the values of 1 or 0 corresponding to solid or fluid domain nodes, respectively. The force between each fluid and the wall can be determined by parameter G_{ads}. The value of G_{ads} is dependent on the contact angle and G_c.

4. Model verification

The available experimental data for steady and transient behaviors of droplets are used to verify the present model's predictions.

4.1. Steady behavior

In this section, the shape of the droplet in various Reynolds numbers has been investigated. The data of Gupta and Basu [17] are used to verify the current LBM results. They have studied the deformation of a droplet adhered to the wall of a rectangular channel experimentally as well as by a commercial CFD code. Their 2D numerical analysis could adequately predict the droplet behavior.

The current study shows that the Aniline droplet deforms and moves along the wall gradually until the shape of the droplet becomes stable. It corresponds to the situation where the advancing and receding contact angles do not change along the flow and remain constant.

Figure 2 demonstrates the stable shape of an Aniline droplet under various flow conditions. The results of Gupta and Basu [17] are shown alongside the current results for the sake of comparison. The volume of the droplet is considered to be 60 µL. First, the flow is assumed to be at rest to calculate the primary shape of the droplet. The contact angle is found to be within 2 % error of the experimental result of Gupta and Basu ($\theta_e=129^o$) [17]. This can be considered as good agreement with the experiments. Then, three different volumetric flow rates have been examined. Reynolds numbers corresponding to various flow rates are 119, 179, and 298. As shown in Figure 2 and other case studies not shown here, in many cases, the shapes of the droplet obtained by the current LBM code demonstrate more resemblance to the experiments than those obtained by the commercial CFD code such as those of Gupta et al. [17].

4.2. Transient behavior

Figure 3 and Figure **4** show the variations of the shape of Aniline and Isoquinoline droplets along the flow, respectively. The volumetric flow rate is Q=12 Lpm. In both figures, the evolution of the droplet shape has been shown in five steps from t=0 s to t=120 ms. As can be seen, the LBM results of the present study are in reasonable agreement with the experiments [17]. It is worthwhile to note that the difference observed in the behavior of the droplets in Figure 3 and Figure **4** is due to the fact that an Isoquinoline droplet has higher wetting characteristics (θ_e=84^o**)** than an Aniline droplet (θ_e=129^o). As shown, the current LBM model provides more accurate results compared to the commercial CFD code.

(a) (b) and (c)

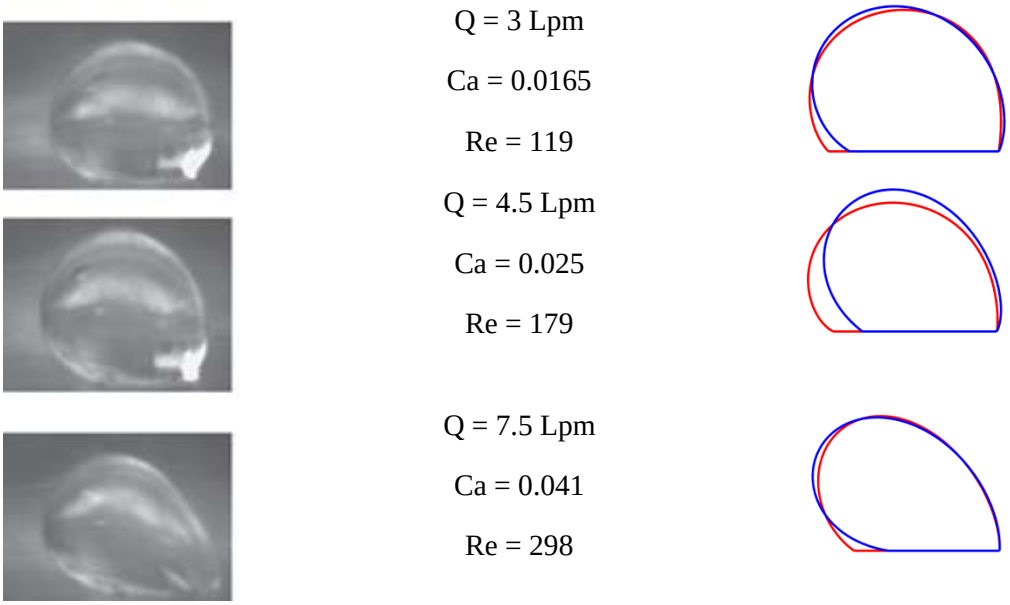

Figure 2. Steady shape of a 60 µL Aniline droplet at different flow rates obtained by: (a) experiment, (b) commercial CFD code, and (c) the present LBM code.

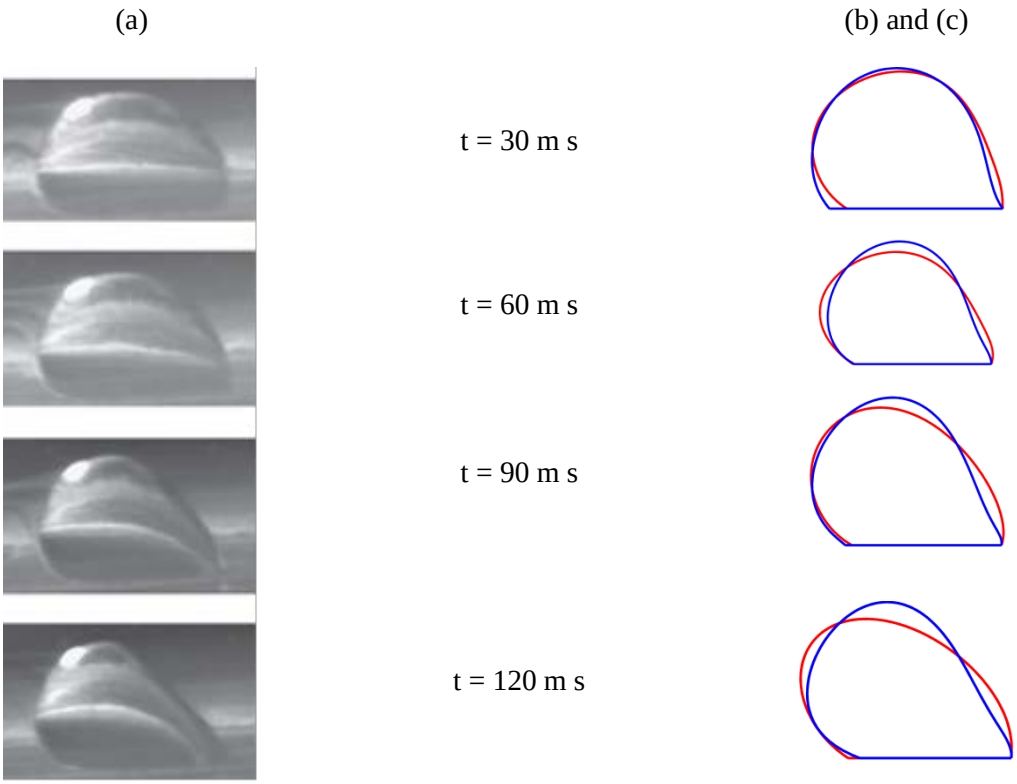

Figure 3. Deformation of a 60µL Aniline droplet with time at *Q*=12 Lpm, *Re*=478, *Ca*=0.066, *Bo*=0.375: (a) visually observed, (b) commercial CFD code, and (c) the present LBM code.

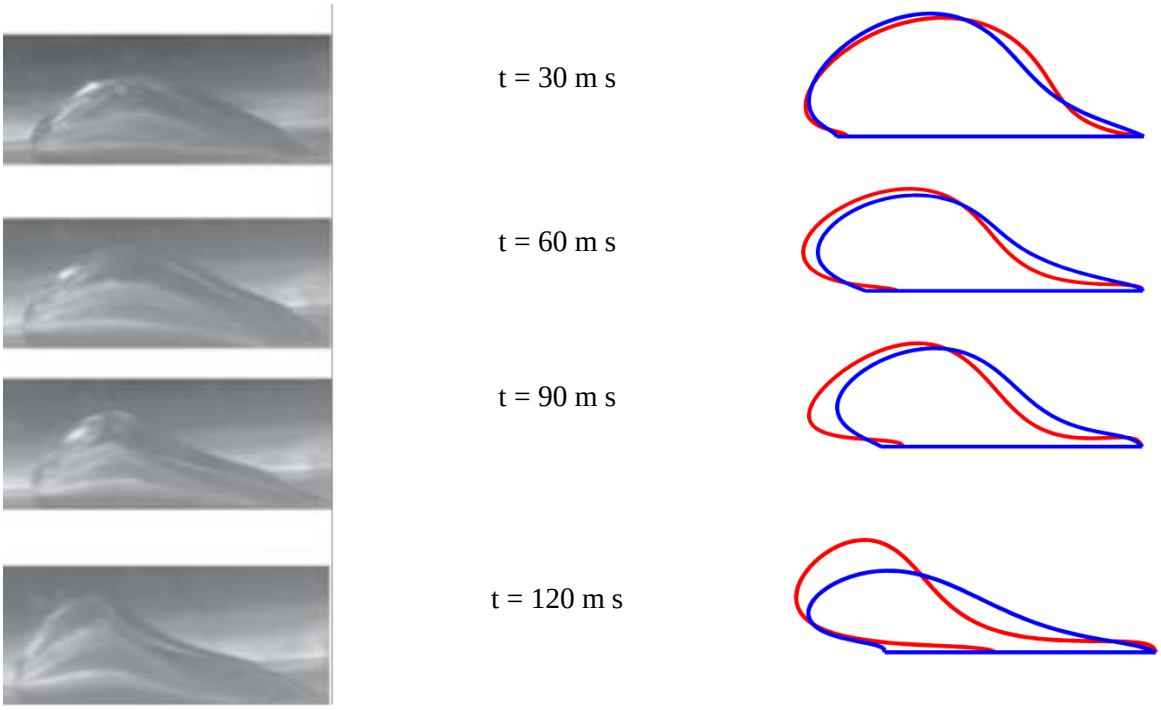

Figure 4. Deformation of a 60µL Isoquinoline droplet with time at *Q*= 12 Lpm, *Re* = 776, *Ca* = 0.497 and *Bo* = 26.3: (a) visually observed, (b) commercial CFD code and (c) the present LBM code.

5. Results and discussion

The results obtained by the current LBM code are presented in two sections corresponding to the crawling and detachment of droplet. The deformation of the droplet in sequential images leading to the detachment of the droplet from the surface has been also captured and demonstrated.

5.1. Crawling of droplet

In this section, the influences of parameters, such as the Reynolds number and the droplet volume, on the crawling of the droplet over the channel surface are studied. The crawling may be explained in terms of positions of the advancing and receding edges of the droplet. The middle point between the advancing and receding edges is assigned to represent the position of the droplet on the surface. Figure 5(a) shows the position of an Aniline droplet, and Figure 5(b) shows the position of the advancing and receding edges for different Reynolds numbers. The droplet volume is 60 µL. It can be seen from Figure 5(a) that as the Reynolds number gets larger, the crawling distance of the droplet increases for the same time intervals. It can be seen from Figure 5(b) that the difference between the positions of advancing and receding edges, proportional to the contact surface between the wall and droplet, reduces during crawling. This process occurs faster as the Reynolds number increases.

Besides the position of the droplet during crawling, it is useful to watch the droplet deformation in the course of the flow. Consequent images of an Aniline droplet starting from t=0 ms to t=2708 ms are shown in Figure 6. The initial contact angle and droplet volume are 110^{o} and 45 µL, respectively. The flow Reynolds number is 200.

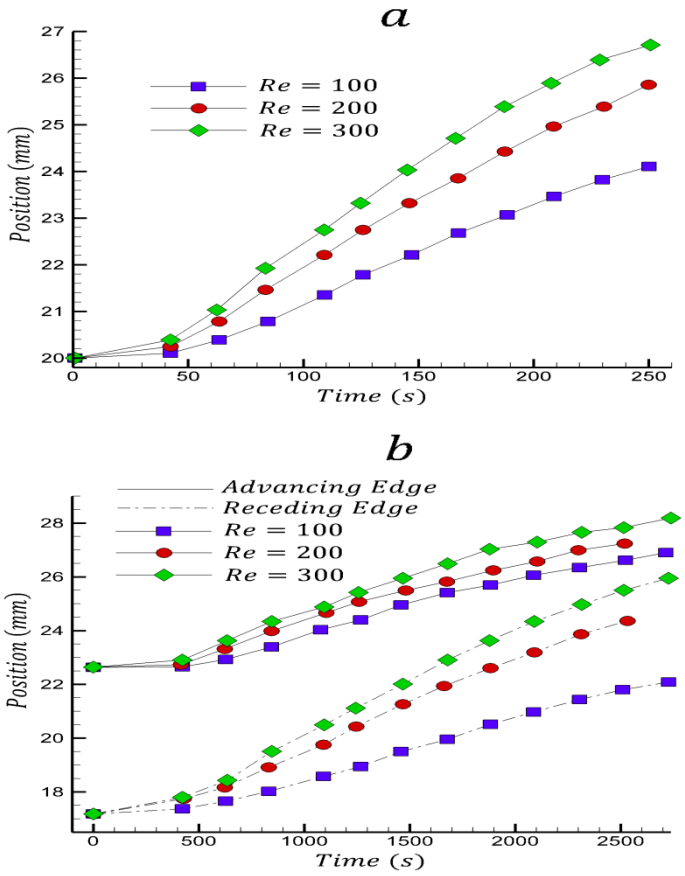

Figure 5. Influence of Reynolds number in sliding step of droplet deformation, V =60µL, (a) position of the droplet in Re = 100, 200, 300, (b) Position of the advancing and receding edges of the droplet in different Reynolds numbers.

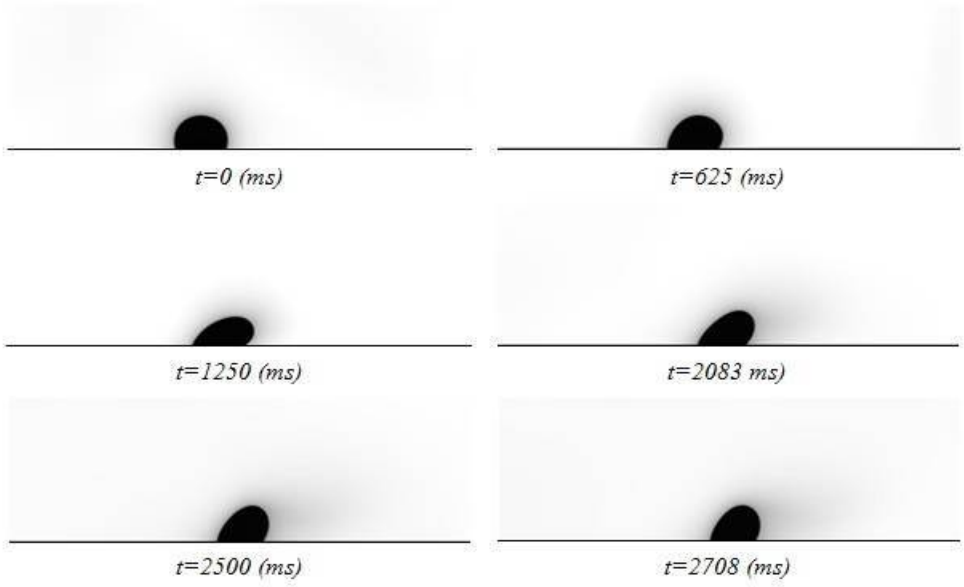

Figure 6. Deformation of an Aniline droplet with θ_e = 110°, V = 45µL and Re = 200.

5.2. Droplet detachment

The shear rate reaches its critical value when the oil droplet is about to become detached from the surface. The critical shear rate is estimated as *U/h* [17], where U is the average free stream velocity in the channel at the instance of detachment, and h is the height of the droplet as shown in **Error! Reference source not found.**. The interfacial tension between the droplet and the surface tends to keep the droplet attached to the surface. Thus, the oil droplet detaches from the surface when the drag force exerted on the oil droplet due to shear flow overcomes the interfacial tension. Figure 7 and Figure **8** show the critical shear rates for different sizes of Isoquinoline and Aniline droplets. It is seen that the critical shear rate decreases with an increase in size of the oil droplet. It is seen that the results of the present LBM solutions are in reasonable agreement with the experiments.

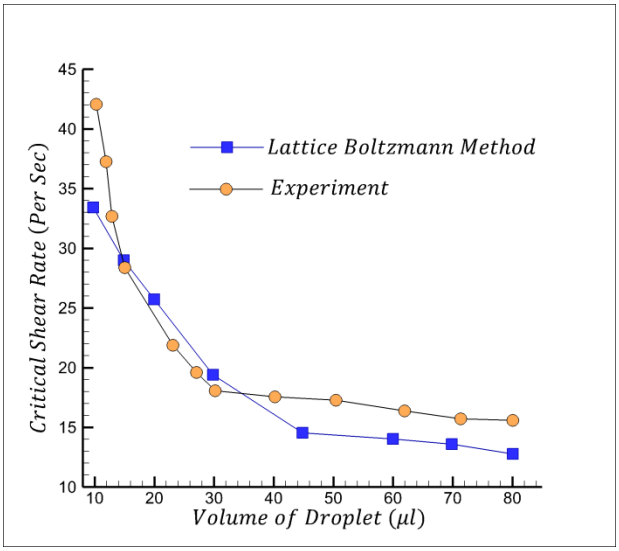

Figure 7. Comparison of the critical shear rates for different sizes of an Isoquinoline droplet obtained by the LBM and experiments.

It is also worthwhile to note that the critical shear rate in Figure 7 for an Isoquinoline droplet is larger than that of an Aniline droplet with the same initial size shown in Figure 8. That is because the interfacial tension between the droplet and the flow of water is smaller for Isoquinoline than Aniline. It means that the initial contact surface between the droplet and the wall is larger for Isoquinoline. Therefore, it presents more resistance against the detachment from the surface.

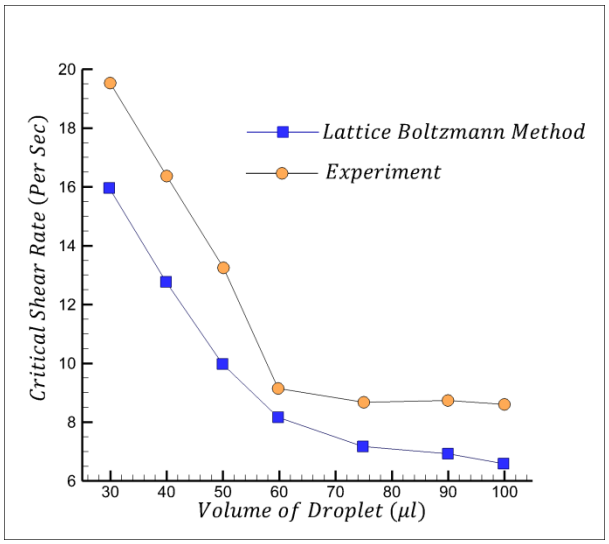

Figure 8. Comparison of the critical shear rates for different sizes of an Aniline droplet obtained by the LBM and experiments.

The droplet deformation leading to the detachment of the droplet from the surface has been investigated. The sequential image shown in Figure 9 demonstrates the gradual deformation of an Aniline droplet with an initial contact angle of 129^{o}. The initial droplet volume is 45μL, and the Reynolds number of the shear flow is considered to be 350. The channel has been taken to be long enough to let the detachment of the droplet occur. As shown in Figure 9, the droplet detaches after about 2083 ms from the start of the flow.

As mentioned earlier, it is obvious that the droplet detaches from the surface once the advancing and receding edges reach each other. The variations of the advancing and receding contact angles in the above example

are shown in Figure 10. Note that the advancing and receding edges overlap at the moment of droplet detachment so that the advancing and receding contact angles become complementary angles.

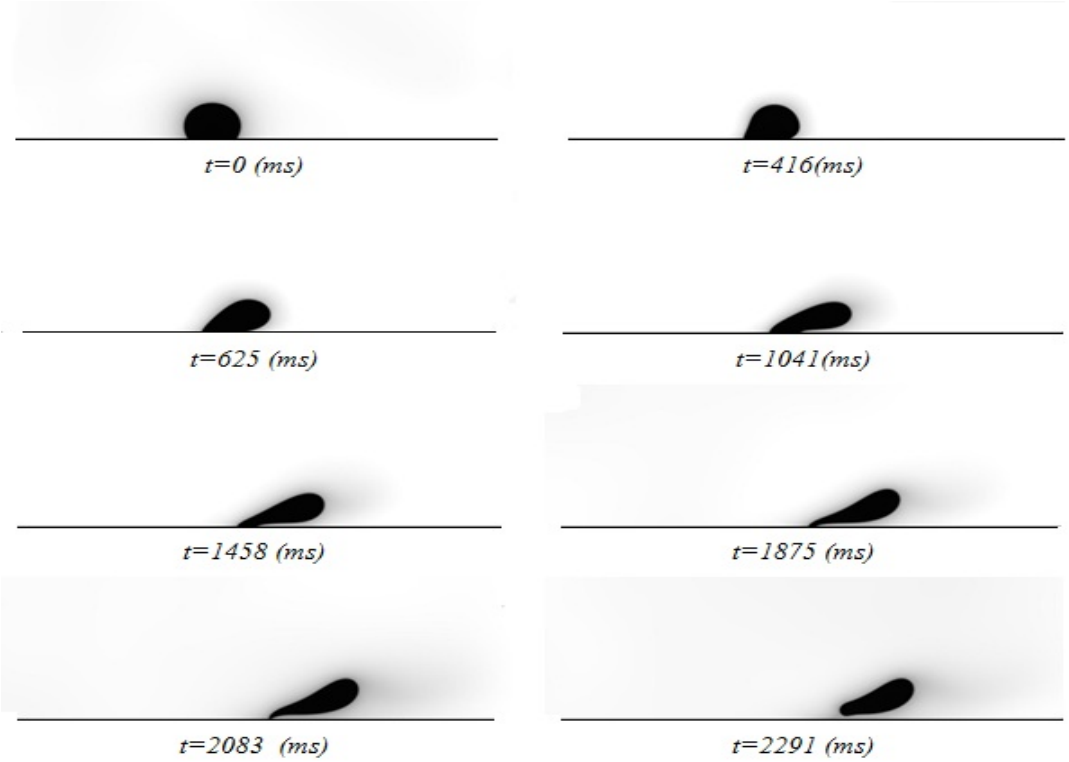

Figure 9. Sequential images of an Aniline droplet in a flow with *Re*=350 demonstrating the gradual deformation from initial conditions (θ_e=129°, *V*=45μL) until droplet detachment.

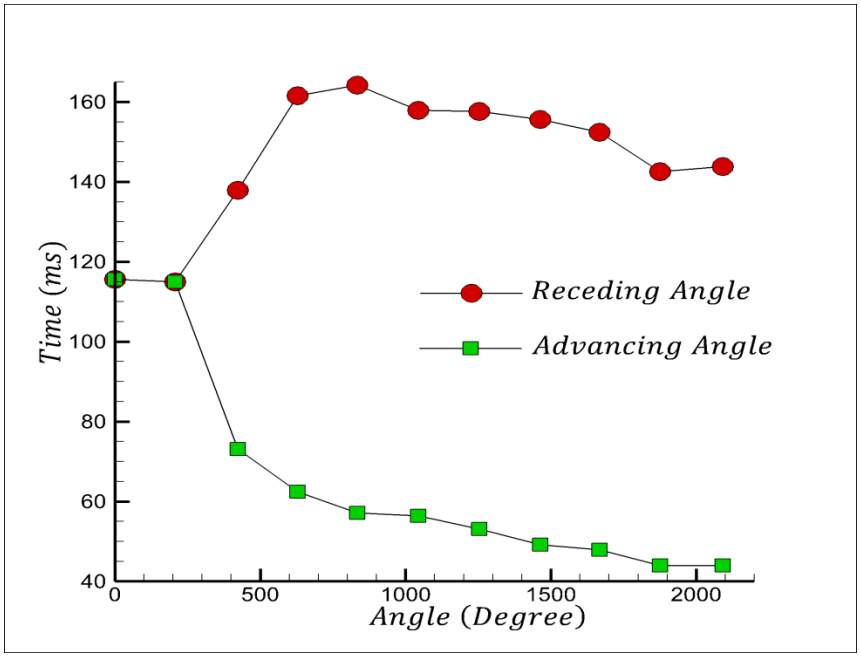

Figure 10. Contact angle hysteresis in the detachment process of an Aniline droplet with θ_e=129°, V=45μL and Re=350.

Under flow and droplet conditions investigated in the above example, the droplet keeps its

entity during the whole process of deformation and detachment. Note, however, that, under certain circumstances, such as for droplets with large adhesive properties and/or low interfacial tensions between the droplet and the flow, the detachment of the droplet may be accompanied by the breakdown of the droplet into two or more parts. One of the torn pieces of the droplet usually tends to remain attached to the wall. To better show this process, sequential images of an Isoquinoline droplet with the initial contact angle of 90^o and the initial volume of 45 µL in a flow with Re=600 are illustrated in Figure 11. The detachment occurs before t=2500 ms.

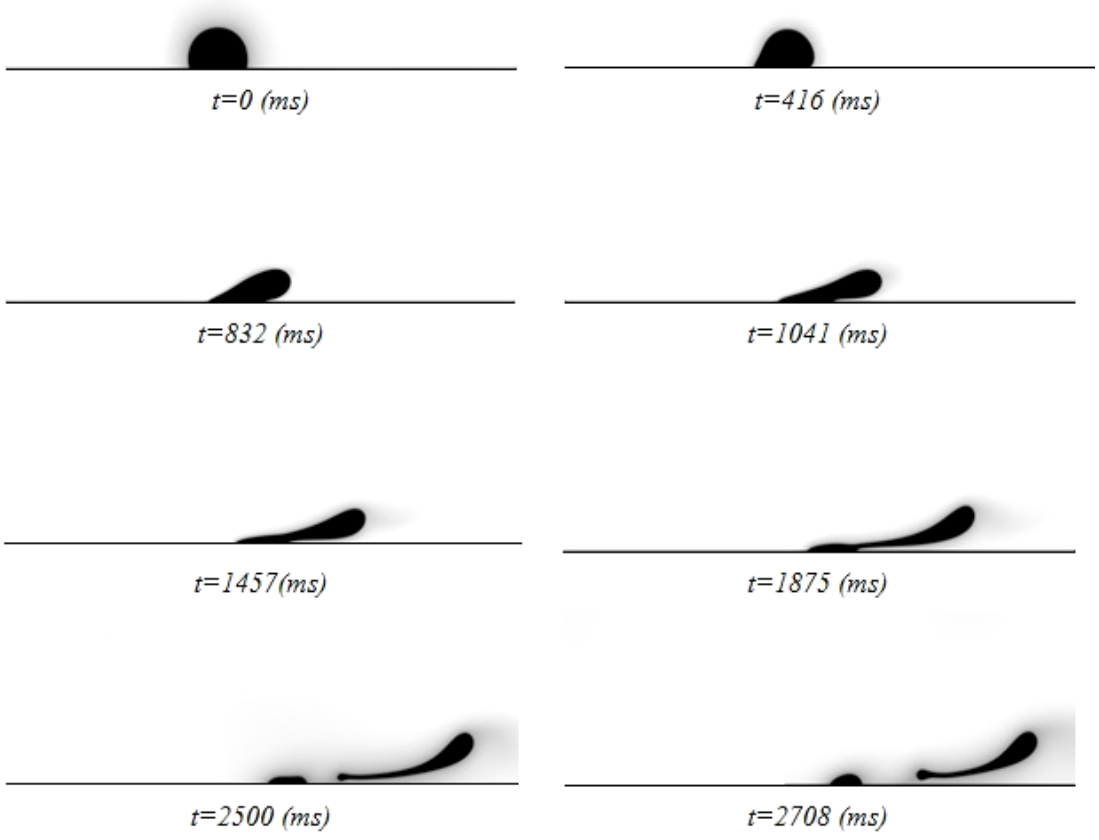

Figure 11. Image sequence of the droplet detachment process of Isoquinoline with θ_e=90^o, V = 45µL and Re = 600.

6. Conclusions

Dynamic deformation of a droplet adherring to the wall which includes sliding, crawling, and detachment in a laminar channel flow was considered. The droplet behaviour was simulated by an LBM scheme using the Shan and Chen model. The influences of Reynolds and Capillary numbers as well as the droplet initial volume on the droplet deformation were investigated. Using two different fluids (Aniline and Isoquinoline) for droplets further highlighted the effects of parameters such as density ratio, viscosity ratio, droplet contact angle, and interfacial tension on the dynamics of droplet deformation. The main conclusions derived are as follows:

1. Before the flow starts, the calculated contact angle is found to be within 2 to

4 % error with respect to experimental results for various droplet initial conditions.

2. The results of the current LBM code confirm that, during the crawling stage, the distance between the advancing and receding edges reduces along the flow until it reaches a constant value. This distance, as well as the distance crawled by the droplet until it reaches its steady shape, decrease as the Reynolds number increases. Further increase of the Reynolds number brings the advanced and receded edges closer together, which is synonymous with the detachment of the droplet from the surface.
3. The predicted shapes of the droplet in various stages of deformation in the course of the flow by the current LBM code demonstrate more resemblance to the experiments than to those obtained by a commercial CFD code.
4. It is observed that, for relatively small droplets, the critical shear rate decreases with the increase in the volume of the oil droplet. However, there is a limiting value for the droplet volume beyond which the critical shear rate remains almost constant and does not demonstrate much correlation with the size of the droplet.
5. Under the flow conditions investigated, wherever the Aniline droplet detaches from, the entire droplet separates from the surface. This is not the case for the Isoquinoline droplet. While the main body is detached, a small part of the Isoquinoline droplet remains attached to the surface in flows with low Reynolds numbers.

References

[1] Inamuro, T., Yoshino, M. and Ogino, F., "Lattice Boltzmann simulation of flows in a three-dimensional porous structure", *International Journal for Numerical Methods in Fluids*, **29** (7), 737 (1999).

[2] He, X., Chen, S. and Zhang, R., "A lattice Boltzmann scheme for incompressible multiphase flow and its application in simulation of Rayleigh–Taylor instability", *Journal of Computational Physics*, **152** (2), 642 (1999).

[3] Eggels, J. G., "Direct and large-eddy simulation of turbulent fluid flow using the lattice-Boltzmann scheme", *International Journal of Heat and Fluid Flow*, **17** (3), 307 (1996).

[4] Martys, N. S. and Chen, H., "Simulation of multicomponent fluids in complex three-dimensional geometries by the lattice Boltzmann method", *Physical Review, E*, **53** (1), 743 (1996).

[5] Charcosset, C., Limayem, I. and Fessi, H., "The membrane emulsification process: A review", *Journal of Chemical Technology and Biotechnology*, **79** (3), 209 (2004).

[6] Thoreau, V., Malki, B., Berthome, G., Boulange-Petermann, L. and Joud, J., "Physico-chemical and dynamic study of oil-drop removal from bare and coated stainless-steel surfaces", *Journal of Adhesion Science and Technology*, **20** (16), 1819 (2006).

[7] Chatterjee, J., "A criterion for buoyancy induced drop detachment based on an analytical approximation of the drop shape", *Colloids and Surfaces, A: Physicochemical and Engineering Aspects*, **178** (1), 249 (2001).

[8] Theodorakakos, A., Ous, T., Gavaises, M., Nouri, J., Nikolopoulos, N. and

Yanagihara, H., "Dynamics of water droplets detached from porous surfaces of relevance to PEM fuel cells", *Journal of Colloid and Interface Science*, **300** (2), 673 (2006).

[9] Lipowsky, H., Riedel, D. and Shi, G., "In vivo mechanical properties of leukocytes during adhesion to venular endothelium", *Biorheology*, **28** (1-2), 53 (1990).

[10] Dimitrakopoulos, P. and Higdon, J., "On the displacement of three-dimensional fluid droplets from solid surfaces in low-Reynolds-number shear flows", *Journal of Fluid Mechanics*, **377**, 189 (1998).

[11] Ding, H. and Spelt, P. D., "Onset of motion of a three-dimensional droplet on a wall in shear flow at moderate Reynolds numbers", *Journal of Fluid Mechanics*, **599**, 341 (2008).

[12] Mahé, M., Vignes-Adler, M., Rousseau, A., Jacquin, C. and Adler, P., "Adhesion of droplets on a solid wall and detachment by a shear flow: I. Pure systems", *Journal of Colloid and Interface Science*, **126** (1), 314 (1988).

[13] Basu, S., Nandakumar, K. and Masliyah, J. H., "A model for detachment of a partially wetting drop from a solid surface by shear flow", *Journal of Colloid and Interface Science*, **190** (1), 253 (1997).

[14] Seevaratnam, G., Ding, H., Michel, O., Heng, J. and Matar, O., "Laminar flow deformation of a droplet adhering to a wall in a channel", *Chemical Engineering Science*, **65** (16), 4523 (2010).

[15] Dussan, V., "On the ability of drops to stick to surfaces of solids, Part 3: The influences of the motion of the surrounding fluid on dislodging drops", *Journal of Fluid Mechanics*, **174**, 381 (1987).

[16] Hao, L. and Cheng, P., "Lattice Boltzmann simulations of liquid droplet dynamic behavior on a hydrophobic surface of a gas flow channel", *Journal of Power Sources*, **190** (2), 435 (2009).

[17] Gupta, A. and Basu, S., "Deformation of an oil droplet on a solid substrate in simple shear flow", *Chemical Engineering Science*, **63** (22), 5496 (2008).

[18] Shan, X. and Chen, H., "Lattice Boltzmann model for simulating flows with multiple phases and components", *Physical Review, E*, **47** (3), 1815 (1993).

[19] Becker, J., Junk, M., Kehrwald, D., Thömmes, G. and Yang, Z., "A combined lattice bgk/level set method for immiscible two-phase flows", *Computers & Mathematics with Applications*, **58** (5), 950 (2009).

[20] Varmazyar, M. and Bazargan, M., "Modeling of free convection heat transfer to a supercritical fluid in a square enclosure by the lattice Boltzmann method", *Journal of Heat Transfer*, **133** (2), 022501 (2011).

[21] Bhatnagar, P. L., Gross, E. P. and Krook, M., "A model for collision processes in gases, I: Small amplitude processes in charged and neutral one-component systems", *Physical Review*, **94** (3), 511 (1954).